Naval Research Laboratory

Washington, DC 20375-5320

NRL/MR/5916/93-7175

AN ANALYTICAL MODEL FOR TURBULENCE-INDUCED FLEXURAL NOISE IN LARGE CONFORMAL SONAR ARRAYS

R. E. Montgomery

Naval Research Laboratory
Underwater Sound Reference Detachment
P.O. Box 568337, Orlando, FL 32856-8337

15 April 1993

Approved for public release; distribution unlimited.

REPORT DOCUMENTATION PAGE

Form Approved
OMB No. 0704-0188

1. AGENCY USE ONLY (Leave blank)	2. REPORT DATE	3. REPORT TYPE AND DATES COVERED
	15 January 1993	FINAL

4. TITLE AND SUBTITLE
An Analytical Model for Turbulence-Induced Flexural Noise in Large Conformal Sonar Arrays

5. FUNDING NUMBERS
PE - 63504N
TA - S0223
WU - DN780-137

6. AUTHOR(S)
Robert E. Montgomery

7. PERFORMING ORGANIZATION NAME(S) AND ADDRESS(ES)
NAVAL RESEARCH LABORATORY
UNDERWATER SOUND REFERENCE DETACHMENT
PO BOX 568337
ORLANDO, FL 32856-8337

8. PERFORMING ORGANIZATION REPORT NUMBER
NRL MEMORANDUM REPORT 7175

9. SPONSORING/MONITORING AGENCY NAME(S) AND ADDRESS(ES)
COMMANDER
NAVAL SEA SYSTEMS COMMAND
WASHINGTON, DC 20362-5101

10. SPONSORING/MONITORING AGENCY REPORT NUMBER

11. SUPPLEMENTARY NOTES

12a. DISTRIBUTION/AVAILABILITY STATEMENT
Approved for public release; distribution unlimited.

12b. DISTRIBUTION CODE

13. ABSTRACT *(Maximum 200 words)*

Large-area, hull-mounted conformal sonar arrays typically employ extended sensors that are configured to detect acoustic signals by means of thickness strains that are induced by the incident pressure field. In most cases, extended sensors also have an appreciable sensitivity to strains in the lateral dimensions. Thus, flexure of such a sensor would induce a signal that would not be differentiated from that of a target. This report presents an analytical approach and a general mathematical model for the noise arising from flexure of the array support plate coupled into the array via the lateral sensitivity of the sensor. The excitation that drives the flexure is assumed to be the turbulent boundary layer created by motion of the platform through the external fluid medium. An analytical expression is derived for the equivalent plane wave spectral density for this noise source. The result is expressed in terms of the frequency response function of the plate, the wave number-frequency spectral density of the excitation, and the spatial filtering characteristics of the array. An application is discussed to show that predictions can be obtained in closed form.

14. SUBJECT TERMS			15. NUMBER OF PAGES
Flow Noise	Planar arrays	Sonar	49
Extended sensors	Flexural noise	Wavenumber filtering	16. PRICE CODE

17. SECURITY CLASSIFICATION OF REPORT	18. SECURITY CLASSIFICATION OF THIS PAGE	19. SECURITY CLASSIFICATION OF ABSTRACT	20. LIMITATION OF ABSTRACT
UNCLASSIFIED	UNCLASSIFIED	UNCLASSIFIED	UL

BLANK PAGE

CONTENTS

BLANK PAGE

AN ANALYTICAL MODEL FOR TURBULENCE-INDUCED FLEXURAL NOISE IN LARGE CONFORMAL SONAR ARRAYS

INTRODUCTION

Large-area conformal arrays that can be mounted to the hull of a ship offer unique tactical advantages over towed arrays. The performance of such arrays is usually limited by self-noise and platform noise. In the latter category, the noise induced by the turbulent boundary layer, located near the hull, is a major concern.

Boundary layer turbulence produces a random pressure field that is detected by the array as a noise source. This is the so-called direct path for flow noise. This path for flow noise exists more or less independently of how the sensors are supported and whether or not they are point sensors versus extended sensors. Flow noise degrades the signal-to-noise ratio but can be reduced by using outer decoupler blankets that serve to attenuate the turbulent boundary layer (TBL) pressure field. The use of extended sensors to provide spatial filtering of the flow noise is also an attractive way to diminish flow noise.

Secondary sources for flow-induced noise can also be significant. If the structural support plate (SSP) is relatively lightweight and compliant, then the TBL can induce flexure of the SSP, which then serves as a secondary source of noise. This noise can enter the array via direct flexure of the extended sensors or as acoustic noise radiated by the edges of the SSP. The radiated component has been addressed by other investigators [1-8]. The former source, flexure induced into the sensors, is the focus of this paper.

Manuscript approved 19 January 1993

The problem will be modeled as follows: the SSP, sensor array, and outer decoupler (OD) are considered to constitute a curved, layered shell with water on the OD side and a vacuum on the SSP side. A backing of a vacuum was chosen because it is simple to model and, in addition, it represents a worst-case scenario; i.e., the case in which the SSP is backed by a pressure release baffle. The Corcos [9] model will be used for the TBL pressure spectrum although the theoretical development is applicable to any model of the wall pressure spectral density. This baseline model is illustrated in Fig. 1. The formalism to be developed makes no presumptions about the boundary conditions on the plate. Later we shall assume that the edges are simply supported in order to illustrate a specific application. Numerous analytical studies of shell and plate motion indicate that, for a large shell or plate, simple supports usually give results that accurately reflect the actual response of a plate supported in more complicated ways. The fluid loading on the plate will be included by using a rather simple model developed by Junger and Feit [10]. The validity of this model will be established by comparing the in-water displacements so derived with the more exact predictions of Sandman's model [11].

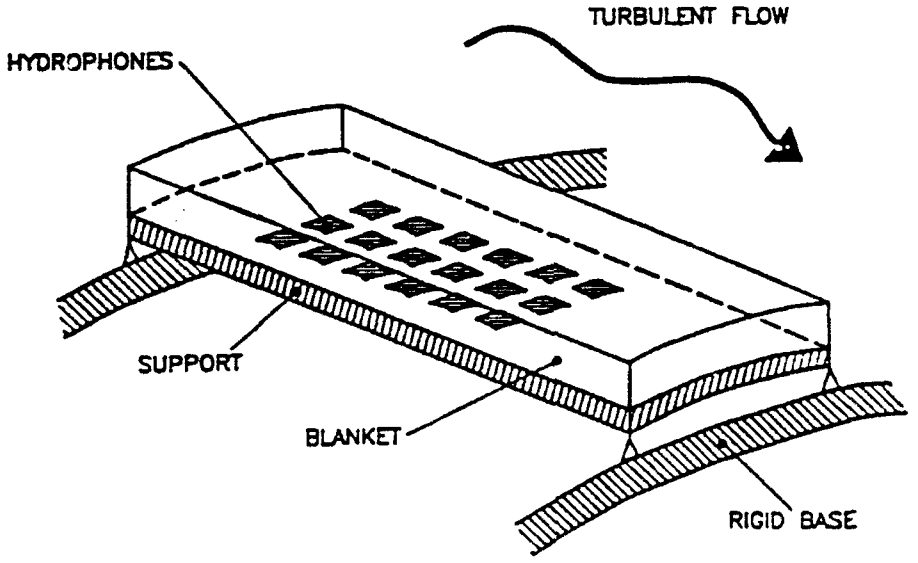

Fig. 1 - Baseline Model

ARRAY RESPONSE TO PLATE FLEXURE

Typically, the extended sensor array is situated on or very near the SSP as shown in Fig. 2. If the plate flexes in response to an external excitation the sensors will follow; therefore, noise will be generated. The external excitation will also be detected by the array even if the plate is rigid; this is the so-called direct path for flow noise discussed earlier. In order to analyze only the flexural contribution, it will be assumed that the sensors do not respond to the direct component.

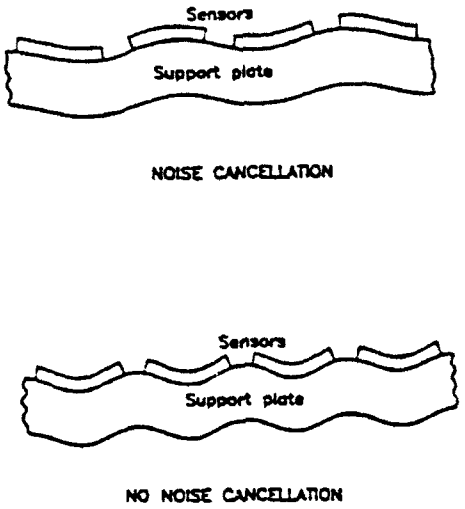

Fig. 2 - Mechanism by which flexural noise is induced into the array

The flexural response of a piezoelectric plate has been modeled by Ricketts [12]. The relevant constitutive equations are

$$T_1 = C_{11}^D S_1 + C_{12}^D S_2 - h_{31} D_3 , \qquad (1a)$$

$$T_2 = C_{12}^D S_1 + C_{22}^D S_2 - h_{32} D_3 , \tag{1b}$$

$$E_3 = -h_{31} S_1 - h_{32} S_2 + \beta_{33}^S D_3 , \tag{1c}$$

and

$$T_3 = T_4 = T_5 = 0 , \tag{1d}$$

where T, S, E, and D represent stress, strain, electric field intensity, and electric displacement, respectively. The matrix components C_{ij}^D, β_{33}^s, and h_{ij} are the elastic, dielectric, and piezoelectric material constants [13]. The superscripts indicate that the designated parameter is held constant.

According to thin plate theory, the strains S_1 and S_2 are related to the displacement of the plate as follows:

$$S_1 = - d \frac{\partial w^2}{\partial x^2} \qquad \text{and} \qquad S_2 = - d \frac{\partial w^2}{\partial y^2} , \tag{2}$$

where d is the distance from the sensor midplane to the neutral plane. S_1 and S_2 are assumed to be constant through the thickness of the sensor hydrophone and D_3 is also constant through the thickness, as can be shown by applying Gauss' law to a dielectric. Consequently, E_3 is constant through the thickness and we can write

$$E_3 = \frac{V}{a} , \tag{3}$$

where V is the voltage between the electrodes and a is the thickness of the sensor.

Assume that the hydrophones are electrically connected in parallel. This is equivalent to steering the array to broadside. Typically, piezoelectric sensors operate in an open circuit mode; hence, the total charge Q_T appearing on the electrodes is zero. Therefore, since D_3 corresponds to the charge density, we can write

$$Q_T = 0 = \sum_{i=1}^{N} \int_{x_i}^{x_i'} \int_{y_i}^{y_i'} D_3 \, dx \, dy \, , \tag{4}$$

where the integrals are performed over the lateral dimensions of each sensor. N denotes the total number of sensors in the array. Using Eq. (1c), we obtain

$$\sum_{i=1}^{N} \int_{x_i}^{x_i'} \int_{y_i}^{y_i'} \left[\frac{V}{a}+h_{31} S_1+h_{32} S_2\right] dx \, dy = 0 \, . \tag{5}$$

The first term is independent of x and y; therefore,

$$\sum_{i=1}^{N} \int_{x_i}^{x_i'} \int_{y_i}^{y_i'} \frac{V}{a} \, dx \, dy = \frac{N \, l_x \, l_y}{a} V \, , \tag{6}$$

where l_x and l_y are the lateral dimensions of an individual sensor. Combining Eq. (5) with Eq. (6) we can write

$$V = \frac{a}{N \, l_x \, l_y} \int_{-\infty}^{\infty} \left[h_{31} S_1+h_{32} S_2\right] A \, (x,y) \, dx \, dy \, , \tag{7}$$

where A (x,y) is an array sensitivity function. For an array composed of unshaded hydrophones we can write

$$A \, (x,y) = \begin{cases} 1 \text{ if } (x,y) \text{ is on a sensor} \\ 0 \text{ if } (x,y) \text{ is not on a sensor} \end{cases} . \tag{8}$$

Equation (7) gives the noise (in volts) that results from a flexural response in terms of the strain components S_1 and S_2. If the external excitation function is deterministic, then there will exist unique, well-defined strains that can be computed with thin plate or shell theories. On

the other hand, if the excitation is a random pressure field (such as TBL), then the displacement and strains must be thought of as stochastic variables, which can be represented by a probability distribution function. In such cases the voltage induced into the array will also be a distributed variable. Therefore, in order to properly assess the noise due to flexure, one must account for the statistical nature of the excitation, which, in our case, is the turbulent boundary layer.

Before proceeding with the development of a stochastic model, it is convenient to express the noise sensed by the array in terms of an equivalent-plane-wave pressure field. This will allow direct comparison of flexural noise with ambient sea noise and other noise specifications. In a free field environment the sensors operate in a hydrostatic mode. An incoming plane wave of amplitude P will produce an electric field, E_3, across the electrodes of a nonflexing sensor of magnitude

$$E_3 = \left(g_{33}+g_{31}+g_{32}\right) P, \tag{9}$$

where g_{33} is the transverse piezoelectric constant, and g_{31} and g_{32} are the lateral piezoelectric constants for a piezoelectric slab that is poled through its thickness. Since E_3 is constant through the thickness, the voltage across the electrodes is $V = E_3 a$. Therefore,

$$V = \left(a g_h\right) P \ , \tag{10}$$

where $g_h = g_{33} + g_{31} + g_{32}$ is known as the hydrostatic g constant. Equation (10) allows the noise, Eq. (7), to be expressed in terms of an equivalent-plane-wave pressure field impinging on an array in the free field.

POWER SPECTRAL DENSITY FOR FLEXURAL NOISE

The spectral density $\Phi_{pp}(\omega)$ for direct flow noise is typically computed by the following relationship:

$$\Phi_{pp}(\omega) = \iint d^2k \; A\,(\vec{k},\vec{k_s},\omega)\; H\,(\vec{k},\omega)\; T\,(\vec{k},\omega)\; P\,(\vec{k},\omega)\;, \qquad (11)$$

where $A\,(\vec{k},\vec{k}_s,\omega)$ is the array function steered to $\vec{k}_s$; $H(\vec{k},\omega)$ is the hydrophone function; $T\,(\vec{k},\omega)$ is the transfer function; and $P(\vec{k},\omega)$ is the wall pressure spectrum. The essential features of the derivation of this relationship are derived in Blake [14] and other references [15-17]. This equation gives the noise level sensed by the thickness mode (3-3 mode); however, for flexure, the noise is induced via an extensional mode. Therefore, Eq. (11) is not appropriate. Starting with the first principles that govern random vibration theory, an analogous expression for flexural noise can be derived. The result will be formally similar to Eq. (11), but the interpretation of the component functions will be quite different.

The following derivation of the power spectral density employs the notation and terminology found in Lin [18].

By combining Eqs. (7) and (10) we can express the equivalent pressure as

$$P(t) = \frac{1}{N g_h\, l_x\, l_y} \int_{-\infty}^{\infty}\int (h_{31}\, S_1 + h_{32}\, S_2)\; A(x,y)\; dx\; dy\;. \qquad (12)$$

As indicated previously, the excitation field is random; therefore, the array output voltage, and hence the equivalent-plane-wave pressure, must be considered as random variables. The transverse displacement w and the lateral strains S_1 and S_2 are also random variables. The power spectral density for the equivalent-plane-wave pressure can be found by taking the

Fourier transform of the corresponding correlation function $R_{pp}(t,t')$ that is defined as

$$R_{pp}(t,t') = E\,[P(t)\,P(t')]\ , \tag{13}$$

where E [ ] indicates the expected value. Because P depends linearly on S_1 and S_2, we obtain from Eq. (12)

$$R_{pp}(t,t') = \left[\frac{1}{Ng_h\, l_x\, l_y}\right]^2 \int\!\!\int_{-\infty}^{\infty} d^2r \int\!\!\int_{-\infty}^{\infty} d^2r' \Big[h_{31}^2\, R_{S_1S_1}(\vec{r},t,\vec{r}',t') \tag{14}$$

$$+ 2\, h_{31}\, h_{32}\, R_{S_1S_2}(\vec{r},t,\vec{r}',t') + h_{32}^2\, R_{S_2S_2}(\vec{r},t,\vec{r}',t')\Big] A(\vec{r})A(\vec{r}')\ ,$$

where $R_{S_1S_1}$, $R_{S_1S_2}$ and $R_{S_2S_2}$, are the cross correlations on strains.

For example,

$$R_{S_1S_2}(\vec{r},t,\vec{r}',t') = E\left[S_1(\vec{r},t)\ S_2(\vec{r}',t')\right]\ . \tag{15}$$

Let $h(\vec{r},\vec{r}',t,t')$ denote the impulse response function of the plate, which is defined as the displacement of the plate at $\vec{r},t$ due to an impulsive load given by

$$P_I(r,t) = \delta(\vec{r}-\vec{r}')\ \delta(t-t') \tag{16}$$

that is applied at $\vec{r}',t'$. The principle of causality requires that $h(\vec{r},\vec{r}',t,t')$ be zero when $t < t'$. A general excitation can be represented by a superposition of impulses; likewise, the displacement can be

represented as a superposition of impulse responses when the system is linear. In addition, h will depend only on the difference $t-t'$. Thus, we can write

$$w(\vec{r}, \vec{t}) = \int_0^t d\tau \iint_R d^2 \vec{r}' \; h(\vec{r}, \vec{r}', t-\tau) \; P(\vec{r}', \tau) \; , \tag{17}$$

where P is the applied pressure and R is the region occupied by the plate. The in-plane strains are, therefore,

$$S_1(\vec{r}, t) = - d \frac{\partial^2 w}{\partial x^2} = - d \int_0^t d\tau \int_R \int d^2 r' \; h_{xx}(\vec{r}, \vec{r}', t-\tau) P(\vec{r}', \tau) \tag{18}$$

and

$$S_2(\vec{r}, t) = - d \frac{\partial^2 w}{\partial y^2} = - d \int_0^t d\tau \int_R \int d^2 r' \; h_{yy}(\vec{r}, \vec{r}', t-\tau) P(\vec{r}', \tau) \; , \tag{19}$$

where $h_{xx} = \partial^2 h/\partial x^2$ and $h_{yy} = \partial^2 h/\partial y^2$.

Using Eqs. (18) and (19), the correlation functions for strains [18] can be written as

$$R_{S_1 S_1}(\vec{r}, t, \vec{r}', t') = d^2 \int_0^t d\tau \int_0^{t'} d\tau' \int_R \int d^2 s \int_R \int d^2 s' \; h_{xx}(\vec{r}, \vec{s}, t-\tau) \tag{20}$$

$$\cdot \; h_{xx}(\vec{r}', \vec{s}', t'-\tau') \; R_{pp}(\vec{s}, \tau; \vec{s}', \tau') ,$$

where R_{pp} is the correlation on pressure. A similar expression is found for $R_{S_1 S_2}$ and $R_{S_2 S_2}$. The cross spectral densities are obtained from the

Fourier transforms of the correlation functions. For example, the cross spectral density for S_1 is given by

$$\Phi_{S_1S_1}(\vec{r}, \omega, \vec{r}', \omega') = \left(\frac{1}{2\pi} \right)^2 \int_{-\infty}^{\infty} \int_{-\infty}^{\infty} R_{S_1S_1}(\vec{r}, t; \vec{r}', t') \cdot \exp^{-i(\omega t - \omega' t')} \, dt \, dt' \,. \tag{21}$$

Assuming the excitation to be weakly stationary, the correlation function for the wall pressure will depend only on the temporal separation $t-t'$. In this case, it can be shown [18] that the correlation functions for the responses also depend only on the temporal separation. Subsequently, the cross spectral densities depend only on a single frequency parameter. Thus, for stationary excitations, Eqs. (20) and (21) may be combined to yield

$$\Phi_{S_1S_1}(\vec{r}, \vec{r}', \omega) = d^2 \int_R \int d^2\vec{s} \int_{R'} \int d^2\vec{s}' \, \Phi_{pp}(\vec{s}, \vec{s}', \omega) \, H_{xx}(\vec{r}, \vec{s}, \omega) \cdot H^*_{x'x'}(\vec{r}', \vec{s}', \omega) \,. \tag{22}$$

Similarly,

$$\Phi_{S_1S_2}(\vec{r}, \vec{r}', \omega) = d^2 \int_R \int d^2\vec{s} \int_{R'} \int d^2\vec{s}' \, \Phi_{pp}(\vec{s}, \vec{s}', \omega) \, H_{xx}(\vec{r}, \vec{s}, \omega) \cdot H^*_{y'y'}(\vec{r}', \vec{s}', \omega) \,, \tag{23}$$

where the frequency influence function $H(\vec{r},\vec{s},\omega)$ is defined as

$$H(\vec{r}, \vec{s}, \omega) \equiv \int_{-\infty}^{\infty} h(\vec{r}, \vec{s}, t) \, e^{-i\omega t} \, dt \,, \tag{24}$$

and Φ_{pp} is the Fourier transform of R_{pp} with respect to time. The subscripts on H denote partial derivatives with respect to $\vec{r}$ or $\vec{r}'$.

For spatially homogeneous excitations, Φ_{pp} will depend only on the spatial separation. In this case, we can replace the integrands of Eqs. (22) and (23) by their spatial Fourier transforms to obtain

$$\Phi_{S_1S_1}(\vec{r}, \vec{r}', \omega) = d^2 \int_{-\infty}^{\infty} \int \Psi_{pp}(\vec{k}, \omega)\, G_{xx}(\vec{r}, \vec{k}, \omega) \cdot G^*_{x_1 x}(\vec{r}', \vec{k}, \omega)\, d^2k \,, \tag{25}$$

where

$$\Psi_{pp}(\vec{k},\omega) = \left(\frac{1}{2\pi}\right)^2 \int_{-\infty}^{\infty}\int \Phi_{pp}(\vec{s}-\vec{s}',\omega) e^{-i\,\vec{k}\cdot(\vec{s}-\vec{s}')}\, d(\vec{s}-\vec{s}') \,,$$

and (26)

$$G_{xx}(\vec{r}, \vec{k}, \omega) = \int_R \int H_{xx}(\vec{r}, \vec{s}, \omega)\, e^{i\,\vec{k}\cdot\vec{s}}\, d^2\vec{s} \,.$$

Similar expressions are obtained for $\Phi_{S_2S_2}$ and $\Phi_{S_1S_2}$. The function $G(\vec{r},\vec{k},\omega)$ is called the sensitivity function. It represents the structural response at point $\vec{r}$ when the excitation is harmonic, having wave number $\vec{k}$ and frequency ω.

For linear structures, Lin [18] and Strawderman [3] have shown that the sensitivity function may be written as a superposition of normal modes. Using the method of Lin, we obtain

$$G_{xx}(\vec{r},\ \vec{k},\ \omega) = \left\{ \sum_{m=1}^{\infty} \frac{\partial^2 f_m(\vec{r})}{\partial x^2}\ S_m\ (\vec{k})\ H_m(\omega)\ \text{for}\ \vec{r}\epsilon R \right\},$$
$$0\ \text{for}\ \vec{r}\epsilon R \qquad (27)$$

where $f_m(\vec{r})$ = normal mode m for the plate *in vacuo*, and

$$S_m(\vec{k}) = \int\int_R f_m\ (r)\ e^{i\ \vec{k}\cdot\vec{r}}\ d^2r. \qquad (28)$$

The frequency response of mode m, $H_m(\omega)$, is defined as the modal displacement of the panel when the excitation is a unit harmonic pressure having wave numbers corresponding to mode m. The function $S_m(\vec{k})$ is commonly referred to as the modal shape function. From Eqs. (25) and (27), we get

$$\Phi_{S_1S_1}\ (\vec{r},\ \vec{r}',\ \omega) = d^2 \sum_{m,n}^{\infty} \frac{\partial^2 f_m(\vec{r})}{\partial x^2} \frac{\partial^2 f_n^*(\vec{r}')}{\partial x'^2} H_m^*(\omega)\ H_n(\omega)$$
$$\cdot \int_{-\infty}^{\infty}\int \Phi_{pp}\ (\vec{k},\omega)\ S_m(\vec{k})\ S_n^*\ (\vec{k})\ d^2k\ . \qquad (29)$$

Similarly,

$$\Phi_{S_1S_2}(\vec{r},\ \vec{r}',\ \omega) = d^2 \sum_{m,n}^{\infty} \frac{\partial^2 f_m(\vec{r})}{\partial x^2} \frac{\partial^2 f_n(\vec{r}')}{\partial y'^2} H_m^*(\omega)\ H_n\ (\omega)$$
$$\cdot \int_{-\infty}^{\infty}\int \Phi_{pp}\ (\vec{k},\omega)\ S_m\ (\vec{k})\ S_n^*\ (\vec{k})\ d^2k\ . \qquad (30)$$

Eq. (29) also gives $\Phi_{S_2S_2}$ by replacing $\partial/\partial x$ with $\partial/\partial y$.

Equations (29) and (30) give the cross spectral densities for strains in terms of the modal response of the structure and the wave number frequency spectrum of the excitation. The power spectral density for flexural noise can now be found by combining the Fourier transform of Eq. (14) with Eqs. (29) and (30). Again invoking temporal stationarity, the time Fourier transform of Eq. (14) yields

$$\Phi_{pp}(\omega) = \left[\frac{d}{Ng_h l_x l_y}\right]^2 \int_{-\infty}^{\infty}\int d^2r \int\int d^2r' \left[h_{31}^2 \Phi_{S_1S_2}(\vec{r},\vec{r}',\omega)\right. \tag{31}$$

$$\left. + 2\, h_{31}h_{32}\, \Phi_{S_1S_2}(\vec{r},\vec{r}',\omega) + h_{32}^2\, \Phi_{S_2S_2}(\vec{r},\vec{r}',\omega)\right] A(\vec{r})\, A(\vec{r}') \ .$$

Combining Eqs. (29), (30), and (31) we obtain

$$\Phi_{pp}(\omega) = \left[\frac{d}{Ng_h\, l_x\, l_y}\right]^2 \sum_{m,n} H_m(\omega)\, H_n^*(\omega) \int_{-\infty}^{\infty}\int \Psi_{pp}(\vec{k},\omega) S_m(\vec{k})\, S_n(\vec{k})\, d^2k$$

$$\cdot \int_{-\infty}^{\infty}\int d^2\vec{r} \int_{-\infty}^{\infty}\int d^2\vec{r}' \left[h_{31}^2 \frac{\partial^2 f_m(\vec{r})}{\partial x^2} \frac{\partial^2 f_n(\vec{r}')}{\partial x'^2}\right. \tag{32}$$

$$\left. + h_{32}^2 \frac{\partial^2 f_m(\vec{r})}{\partial y^2} \frac{\partial^2 f_n(\vec{r}')}{\partial y'^2} \right] A(\vec{r})\, A(\vec{r}') \ .$$

If we define $\Phi_{p_{mn}}(\omega) \equiv \int_{-\infty}^{\infty}\int \Psi_{pp}(\vec{k},\omega)\, S_m(\vec{k})\, S_n^*(\vec{k})\, d^2k$, (33)

and
$$a_{mn}(\vec{r}, \vec{r}') \equiv h_{32}^2 \frac{\partial^2 f_m}{\partial x^2} \frac{\partial^2 f_n}{\partial x'^2} + h_{31} h_{32} \frac{\partial^2 f_n}{\partial x'^2} \frac{\partial^2 f_m}{\partial y^2} + h_{31} h_{32} \frac{\partial^2 f_m}{\partial x^2} \frac{\partial^2 f_n}{\partial y'^2} + h_{32}^2 \frac{\partial^2 f_m}{\partial y^2} \frac{\partial^2 f_n}{\partial y'^2}, \tag{34}$$

then Eq. (32) can be written as

$$\Phi_{pp}(\omega) = \left(\frac{d}{N g_h l_x l_y}\right)^2 \sum_{m,n} H_m(\omega) H_n^*(\omega) \Phi_{p_{mn}}(\omega) \int_{-\infty}^{\infty}\int d^2 r \int_{-\infty}^{\infty}\int d^2 r' \, a_{mn}(\vec{r}, \vec{r}') A(\vec{r}) A(\vec{r}') . \tag{35}$$

Equation (35) is the central result of this paper. It provides the formal connection between the wave number-frequency spectral density of the excitation field and the power spectral density for the equivalent-plane-wave pressure sensed by the array. This relationship is the analog of Eq. (11), the formula that is used for direct path flow noise. The term $\Phi_{p_{mn}}$ in Eq. (35) is the analog of the term $P(\vec{k},\omega)$ in Eq. (11). It accounts for the spectrum of the excitation field through the relationship given by Eq. (33), where Ψ_{pp} is identical to $P(\vec{k},\omega)$. The last term in Eq. (35) is the analog of the product of the array and hydrophone functions in Eq. (11). This term accounts for the size and location of the sensors in the array. The terms $H_m(\omega)$ and $H_n^*(\omega)$, called frequency response functions (FRF), are not found in Eq. (11). These terms account for the modal response of the plate to a harmonic excitation; that is, the response to each modal component of pressure in the spectrum of the excitation field. The FRF carries information about the material properties of the plate as well as the effects of water loading and intermodal coupling.

The double sum over modes in Eq. (35) can be thought of as representing a type of intermodal coupling. Thus, one could have two types of intermodal coupling: (1) via the water loading on the plate, and (2) via the off-

diagonal terms in Eq. (35). These off-diagonal terms arise from cross-correlations of normal mode strains.

THE FREQUENCY RESPONSE FUNCTION

The modal frequency response function $H_m(\omega)$ can be found by solving for the steady state motion of the system when a unit-amplitude, harmonic-generalized force in mode m is applied. For a rectangular isotropic thin plate, simply supported and fluid loaded on one side, Lin [18] derives the following frequency response function:

$$H_m(\omega) = \frac{4}{L_x L_y}\left[D\left(k_{m_x}^2 + k_{m_y}^2\right)^2 - \rho\omega^2 - \frac{i\rho_f \omega^2}{\sqrt{k_a^2 - k_{m_x}^2 - k_{m_y}^2}}\right]^{-1}, \quad m = (m_x, m_y), \tag{36}$$

where L_x and L_y are the plate dimensions, ρ is the mass per unit area of the plate, D is the plate flexural rigidity, k_a is the acoustic wave number, and ρ_f is the density of the fluid. The modal wave numbers are given by

$$k_{m_x} = \frac{m_x \pi}{L_x}, \quad m_x = 0, 1, 2, \ldots.$$

and

$$k_{m_y} = \frac{m_y \pi}{L_y} \quad m_y = 0, 1, 2, \ldots. \tag{37}$$

Equation (36) provides a good model for the frequency response function when the mass and stiffness of the isotropic support plate is much greater

than those of the sensors and the outer decoupler. When the support plate is orthotropic, and/or comparable in mass and stiffness to the other components, then the entire structure must be thought of as a composite layered plate or shell. In such cases, the frequency response function may be obtained using the Donnel shell theory as generalized by Dong [19] to include layered shells.

Consider an open shell of N layers as shown in Fig. 3. The boundaries of the shell are defined as x=0, θ=0 and x=x_o, θ=θ_o. The radius of the shell is R. Each layer is homogenous and isotropic. The stress-strain relationship for the k^{th} layer is

$$\begin{bmatrix} \sigma_x^{(k)} \\ \sigma_\theta^{(k)} \\ \tau_{x\theta}^{(k)} \end{bmatrix} = \begin{bmatrix} A_{11}^{(k)} & A_{12}^{(k)} & 0 \\ A_{12}^{(k)} & A_{11}^{(k)} & 0 \\ 0 & 0 & A_{66}^{(k)} \end{bmatrix} \begin{bmatrix} \epsilon_\chi \\ \epsilon_\theta \\ \gamma_{x\theta} \end{bmatrix}, \tag{38}$$

with

$$A_{11}^{(k)} = \frac{E^{(k)}}{1 - \nu^{(k)2}},$$

$$A_{12}^{(k)} = \frac{\nu^{(k)} E^{(k)}}{1 - \nu^{(k)2}}, \tag{39}$$

and

$$A_{66}^{(k)} = \frac{E^{(k)}}{2\left[1+\nu^{(k)}\right]},$$

where E and ν represent Young's modulus and Poisson's ratio.

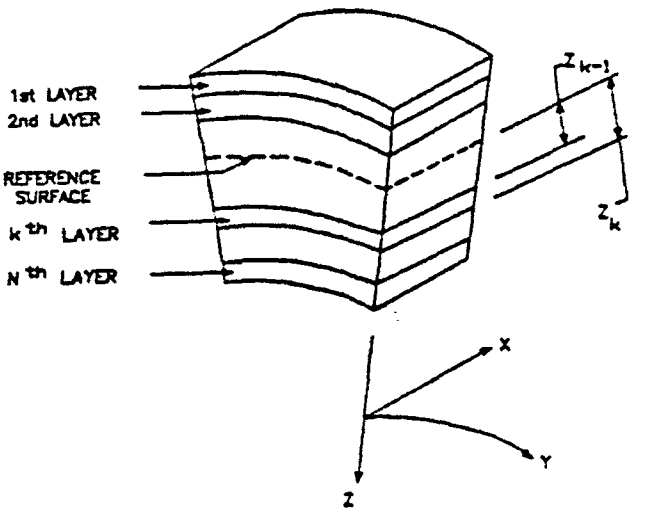

Fig. 3 - Composite shell model

Evaluation of the force-resultant and moment-resultant integrals requires piecewise integration through the thickness. The resulting equations of motion are

$$[\Gamma] \begin{bmatrix} u \\ v \\ w \end{bmatrix} = \begin{bmatrix} q_x \\ q_\theta \\ q_z \end{bmatrix} , \tag{40}$$

where $[\Gamma]$ is a differential operator matrix given by

$$\Gamma_{11} = C_{11} \frac{\partial^2}{\partial x^2} + \frac{C_{66}}{R^2} \frac{\partial^2}{\partial \theta^2} - \rho \frac{\partial^2}{\partial t^2} , \tag{41a}$$

$$\Gamma_{22} = C_{66} \frac{\partial^2}{\partial x^2} + \frac{C_{22}}{R^2} \frac{\partial^2}{\partial \theta^2} - \rho \frac{\partial^2}{\partial t^2} , \tag{41b}$$

$$\Gamma_{33} = \left[D_{11} \frac{\partial^4}{\partial x^4} + \frac{2}{R^2} \left(D_{12}+2D_{66} \right) \frac{\partial^4}{\partial x^2 \, \partial \theta^2} + \frac{D_{22}}{R^4} \frac{\partial^4}{\partial \theta^4} \right] \tag{41c}$$

$$+ \frac{2}{R} \left[D^*_{12} \frac{\partial^2}{\partial x^2} + \frac{D^*_{22}}{R^2} \frac{\partial^2}{\partial \theta^2} + \frac{C_{22}}{R^2} + \rho \frac{\partial^2}{\partial t^2} \right.,$$

$$\Gamma_{12} = \Gamma_{21} = \frac{\left(C_{12}+C_{66} \right)}{R} \frac{\partial^2}{\partial x \, \partial \theta} \,, \tag{41d}$$

$$\Gamma_{13} = \Gamma_{31} = - \frac{C_{12}}{R} \frac{\partial}{\partial x} - D^*_{11} \frac{\partial^3}{\partial x^3} - \left(D^*_{11}+\frac{2D^*_{66}}{R^2} \right) \frac{\partial^3}{\partial x \partial \theta^2} \,, \tag{41e}$$

and

$$\Gamma_{23} = \Gamma_{32} = - \frac{C_{22}}{R^2} \frac{\partial}{\partial \theta} - \frac{D^*_{22}}{R^3} \frac{\partial^3}{\partial \theta^3} - \frac{1}{R} \left(D^*_{12}+2D^*_{66} \right) \frac{\partial^3}{\partial x^2 \, \partial \theta} \,, \tag{41f}$$

where

$$\left(C_{ij}, \, D^*_{ij}, \, D_{ij} \right) = \sum_{k=1}^{N} A^{(k)}_{ij} \left[\left(z_k - z_{k-1} \right), \, \frac{1}{2} \left(z_k^2 - z_{k-1}^2 \right), \right. \tag{42}$$

$$\left. \frac{1}{3} \left(z_k^3 - z_{k-1}^3 \right) \right] \,,$$

$$\rho = \sum_{k=1}^{N} \rho_k \left(z_k - z_{k-1} \right) \,, \tag{43}$$

and ρ_k = Volume density of layer k, R = Shell radius, ρ = Area density of the composite plate and q_x q_θ q_z are surface loads (pressures). All edges are assumed to be supported by shear diaphragms; i.e.,

$$\text{along } x = 0 \text{ and } x = x_o \,, \qquad v = w = 0 \text{ and } N_x = M_x = 0 \,, \tag{44}$$

and

$$\text{along } \theta = 0 \text{ and } \theta = \theta_o \,, \qquad u = w = 0 \text{ and } N_\theta = M_\theta = 0 \,. \tag{45}$$

These boundary conditions are satisfied exactly by choosing displacement functions as follows

$$u = u_o e^{j\omega t} \cos(\lambda s) \sin(n\theta) \,,$$

$$v = v_o e^{j\omega t} \sin(\lambda s) \cos(n\theta) \,, \tag{46}$$

and

$$w = w_o e^{j\omega t} \sin(\lambda s) \sin(n\theta) \,,$$

where u is the displacement in the x direction, v the displacement in the θ direction, and w the displacement in the z direction. Also, s is defined as x/R and

$$\lambda = \frac{m\pi R}{x_o} \quad m = 0, 1, 2....$$

$$n = \frac{k\pi}{\theta_o} \quad k = 0, 1, 2.... \,. \tag{47}$$

In general n is not an integer. The index k is one more than the number of longitudinal node lines along the shell.

Inserting Eq. (46) into Eq. (41), we obtain

$$\Gamma_{11} = - C_{11} \lambda^2 - \frac{C_{66}}{R^2} n^2 + \rho\omega^2 , \tag{48a}$$

$$\Gamma_{22} = - C_{66} \lambda^2 - \frac{C_{11}}{R^2} n^2 + \rho\omega^2 , \tag{48b}$$

$$\Gamma_{33} = D_{11} \lambda^4 + \frac{2}{R^2} \left(D_{12}+D_{66}\right) \lambda^2 n^2 + \frac{D_{11}}{R^4} n^4$$

$$- \frac{2}{R} \left(D^*_{12} \lambda^2 + \frac{D^*_{11}}{R^2} n^2\right) + \frac{C_{11}}{R^2} - \rho\omega^2 , \tag{48c}$$

$$\Gamma_{12} = - \frac{\left(C_{12} + C_{66}\right)}{R} \lambda n , \tag{48d}$$

$$\Gamma_{13} = \frac{C_{12}}{R} \lambda - D^*_{11} \lambda^3 + \left(D^*_{12}+\frac{2D^*_{66}}{R^2}\right) \lambda n^2 , \tag{48e}$$

and

$$\Gamma_{23} = \frac{C_{11}}{R^2} n - \frac{D^*_{11}}{R^3} n^3 + \frac{1}{R} \left(D^*_{12}+2D^*_{66}\right) \lambda^2 n , \tag{48f}$$

writing

$$\begin{aligned} \alpha_{11} &= - \Gamma_{11} & \alpha_{12} &= \Gamma_{12} \\ \alpha_{22} &= - \Gamma_{22} & \alpha_{13} &= - \Gamma_{13} \\ \alpha_{33} &= \Gamma_{33} & \alpha_{23} &= - \Gamma_{23} . \end{aligned} \tag{49}$$

The resonance frequencies of the shell can be found by solving

$$\begin{vmatrix} \alpha_{11} & \alpha_{12} & \alpha_{13} \\ \alpha_{12} & \alpha_{22} & \alpha_{23} \\ \alpha_{13} & \alpha_{23} & \alpha_{33} \end{vmatrix} = 0 . \qquad (50)$$

Model Verification

The natural frequencies of a closed, two-layered cylindrical shell were computed from Eq. (50). The results are identical to Dong's results [19] when the reference surface is taken to be the neutral fiber.

The resonance frequencies of various open shells of one layer of isotropic material have been computed and compared to the Donnel-Mushtari model values reported by Leissa [20]. A partial comparison, Table 1, shows excellent agreement with the Donnel-Mushtari model for a single-layered, isotropic open shell.

Table 1 - Lowest Resonances of a Single Layer Open Shell [20]

x_o 1/mR	Computed Resonance (Hz)	Leissa (Hz)
	n = 1/3	
0.10	14.27821	14.2782
0.25	2.471323	2.47132
1.00	0.9465441	0.946544
4.00	0.422183	0.422183
20.00	5.1433217E-02	5.14333E-02
100.00	2.6873313E-03	2.68829E-03
	n = 1/2	
0.10	14.28020	14.2802
0.25	2.472816	2.47281
1.00	0.9308990	0.930899
4.00	0.3814159	.0381416
20.00	3.6844123E-02	3.68447E-02
100.00	2.3361256E-03	2.32640E-03
	n = 2/3	
0.10	14.28297	14.2830
0.25	2.47491	2.47491
1.00	0.9103304	0.910330
4.00	0.3378275	0.337827
20.00	2.7429942E-02	2.74266E-02
100.00	3.7624016E-03	3.74949E-03

The results given in Table 1 show that the model is consistent with published results that are known to be valid for thin plate or shell

applications. The key question is whether or not the model provides a good representation of a typical support plate/sensor array/outer decoupler for a practical sonar array. An illustrative example, to be discussed further in a subsequent section of this report, consists of a 0.0254m thick cylindrical steel shell overlayed with a 0.0508m thick elastomer blanket. The lateral dimensions are L_x = 4m and L_y = 2m. The radius of curvature of the shell is 5.2 m. The frequency range of interest is 1 kHz to 10 kHz. The material parameters are

Elastomer layer: $E = 1.0 \times 10^6$ Pa $\quad \nu = 0.49 \quad \rho = 1200$ kg/m^3

Steel support: $E = 2.1 \times 10^{11}$ Pa $\quad \nu = 0.3 \quad \rho = 7900$ kg/m^3 .

Many resonances are found in the frequency range of 1 kHz to 10 kHz as shown in Fig. 4. The same computation has been performed for a flat plate having the same size as the structure of interest. Figure 5 shows a comparison of the results for the flat plate and the shallow shell. The differences are significant only for modes having $m_x < 17$ and $m_y < 5$. These modes are below 1 kHz; so, to simplify the model, the curvature of the shell can be neglected. The same conclusions were found to be true for a fiberglass support plate.

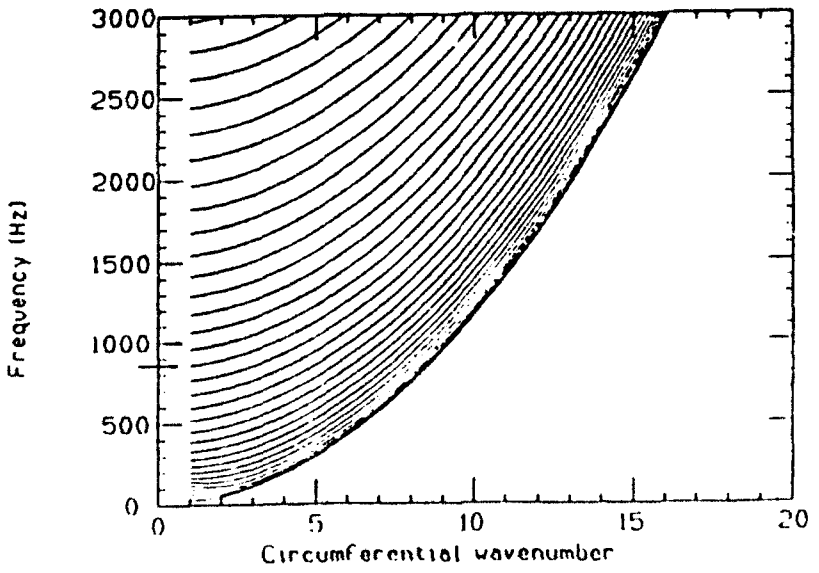

Fig. 4 - Modes of a shallow shell

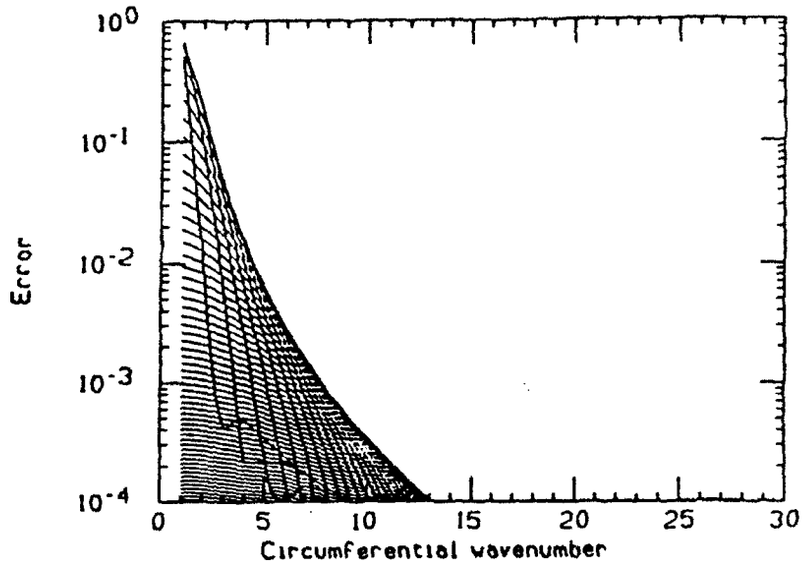

Fig 5. - The relative error, in frequency, incurred setting the shell curvature to zero

As reported by Dong [19], the shallow shell model can be converted to a flat plate model by making the following transpositions:

$$\begin{aligned} &R \to \infty \\ &\theta_o \to 0 \\ &R\theta_o \to L_y, \text{ the length along curved edge.} \end{aligned} \tag{51}$$

The equation of motion Eq. (40) now becomes

$$\Gamma_{33} \cdot w = q_z \ , \tag{52}$$

with

$$\Gamma_{33} = D_{11} \left[k_{m_x}^4 + k_{m_y}^4\right] + 2 \left[D_{12} + 2D_{66}\right] k_{m_x}^2 \, k_{m_y}^2 - \rho\omega^2 \ , \tag{53}$$

and

$$k_{m_x} = \frac{m_x \pi}{L_x} \quad , \; m_x = 0, \; 1, \; 2, \; \ldots .$$
$$k_{m_y} = \frac{m_y \pi}{L_y} \qquad m_y = 0, \; 1, \; 2, \; \ldots . \tag{54}$$

For a single layer of isotropic material these equations reduce to the classical equation of motion for a thin rectangular plate.

Validity of the Thin Plate Assumption

A general criteria for the range of validity of a thin plate model does not exist. The critical frequency proposed by Junger and Feit [10] for a 0.0254-mm thick steel plate is f = 8006 Hz, and even higher for a fiberglass plate. Therefore, a thin plate approximation would seem to be valid below about 8 kHz.

Water Loading and Driving Force

Let q_F denote the forcing function, and let P_a represent the acoustic pressure created in the fluid by the plate motion. Equation (52) becomes

$$\Gamma_{33} \, w = q_F - P_a . \tag{55}$$

We assume that w can be expressed as a sum of *in vacuo* eigenvectors

$$w = \sum_{m_x=1}^{\infty} \sum_{m_y=1}^{\infty} w_{m_x m_y} \sin\left(k_{m_x} x\right) \sin\left(k_{m_y} y\right) . \tag{56}$$

Similarly, q_F and P_a can be expressed as:

$$q_F = \sum_{m_x=1}^{\infty} \sum_{m_y=1}^{\infty} q_{m_x m_y} \sin\left(k_{m_x} x\right) \sin\left(k_{m_y} y\right) , \tag{57}$$

and

$$P_a = \sum_{m_x=1}^{\infty} \sum_{m_y=1}^{\infty} P_{m_x m_y} \sin\left(k_{m_x} x\right) \sin\left(k_{m_y} y\right) \tag{58}$$

to obtain a linear set of equations.

Modal Decomposition of the Forcing Function

The forcing function used in flow noise computation is usually a wall pressure spectrum. The amplitude q_0 depends on the particular model used to represent the spectrum. A given wave number component is equivalent to a forcing function that can be expressed as

$$q_F = q_0 \sin(k_x x) \sin(k_y y) . \tag{59}$$

Following Timoshenko and Woinowsky-Krieger [21], a modal component of $q_{m_x m_y}$, Eq. (57), can be obtained by

$$q_{m_x m_y} = \frac{4}{L_x L_y} \int_0^{L_x} \int_0^{L_y} q_F(x,y) \sin\left(\frac{m_x \pi x}{L_x}\right) \sin\left(\frac{m_y \pi y}{L_y}\right) dxdy . \tag{60}$$

Water Loading Effect

This problem has been studied by many authors [22-26]. Most of the available models have been summarized by Leibowitz [27]. The major complication arising from water loading is that the orthogonal *in vacuo* eigenmodes become intercoupled by the water loading. That is, the interaction of the fluid and plate is a function of all the modes.

We shall adopt the Junger and Feit model as described by Leibowitz [27]; this model was developed for symmetric modes of the plate. However, the analytical result is valid for both symmetric and antisymmetric modes (Leibowitz [27], Table 1).

The Junger and Feit model for the water loading can be decomposed into modal components in the same way as was done for an externally applied pressure [Eq. (60)]. The result for mode (m,n) is

$$P_{mn} = i\omega \sum_{pq} I_{mnpq} w_{pq} , \tag{61}$$

where

$$I_{mnpq} = \frac{\rho\omega k_m k_n (-1)^{m+n}}{\pi^2} \sum_{pq} (-1)^{p+q} k_p k_q \cdot \left[\int_{\omega}^{\infty} \int \frac{\mathrm{Cos}^2 \gamma_x L_x \, \mathrm{Cos}^2 \gamma_y L_y \, d\gamma_x d\gamma_y}{\left(k^2-\gamma_x^2-\gamma_y^2\right)^{1/2} \left(k_m^2-\gamma_x^2\right)\left(k_n^2-\gamma_y^2\right)\left(k_p^2-\gamma_x^2\right)\left(k_q^2-\gamma_y^2\right)} \right] \tag{62}$$

$$= \left(r_{mnpq} - i\omega m_{mnpq}\right) L_x L_y / 4$$

and

$$r_{mnpq} = \mathrm{Re}\left[I_{mnpq}\right]$$
$$m_{mnpq} = -\frac{1}{\omega} \mathrm{Imag}\left[I_{mnpq}\right] . \tag{63}$$

By examination of Eq. (61) we see that each mode (m,n) is coupled to all of the other modes via the term I_{mnpq}.

Cross Coupling

Leibowitz [27] has shown that the cross coupling terms are much smaller than the self-impedance components when $k_a L_x$ and $k_a L_y$ >3, which for $\omega << \omega_c$ is equivalent to $k_{m_x} L_x$ and $k_{m_y} L_y$ >>1 (the thin plate criteria). Here k_a is the acoustic wave number ω/c. This criteria is satisfied for the SSP over the frequency band of interest. Moreover, Sandman [11] has shown that when moderate structural damping is included, the cross coupling terms are negligible. For reassurance, cross coupling terms were computed numerically and were found to be negligible for the problem of interest.

Approximate Water Loading

When cross terms are negligible, as is the case for the SSP, the equivalent modal pressure on the plate can be expressed as [10]

$$P_{m_x m_y} \approx \frac{i \rho_f \omega^2 w_{m_x m_y}}{\sqrt{k_a^2 - k_{m_x}^2 - k_{m_y}^2}} , \qquad (64)$$

where ρ_f is the density of water and k_a is the acoustic wave number.

As a final check on this approximation, some typical modes were computed and the results compared to the more exact results obtained by numerical integration of Eq. (62). A representative comparison is shown in Table 2 for 8 kHz, where the agreement is expected to be the worst. The differences between the approximate values and the exact values are found to lead to errors of no more than 1 dB in the final result.

Table 2 - Water Loading: Comparison of Approximate and Exact Methods

Frequency = 8000 Hz		
I_{mngr}	Approximate (Ns/m)	Exact (Ns/m)
$I_{11\ 11}$	1.368×10^7	$(1.357 \times 10^7 - j\ 1.666 \times 10^6)$
$I_{20\ 20\ 20\ 20}$	7.687×10^7	$(5.208 \times 10^7 - j\ 2.671 \times 10^7)$
$I_{21\ 21\ 21\ 21}$	$j5.222 \times 10^7$	$(2.160 \times 10^7 + j\ 4.963 \times 10^7)$
$I_{30\ 30\ 30\ 30}$	$j1.253 \times 10^7$	$(3.281 \times 10^7 + j\ 1.162 \times 10^7)$

Flexural Response of the SSP

Substituting Eqs. (53), (56), (57), and (64) into Eq. (55) leads to an infinite set of uncoupled equations

$$\left[D_{11} \left(k_{m_x}^6 + k_{m_y}^6 \right) + 2 \left(D_{12} + 2\, D_{66} \right) k_{m_x}^2 k_{m_y}^2 - \rho \omega^2 - \frac{i \rho_f \omega^2}{\sqrt{k_a^2 - k_{m_x}^2 - k_{m_y}^2}} \right] w_{m_x m_y} = q_{m_x m_y} - P_{m_x m_y} \,. \tag{65}$$

The total displacement can then be found by summing over modes, as

$$w = \sum_{m_x=1}^{\infty} \sum_{m_y=1}^{\infty} w_{m_x m_y} \sin \left(k_{m_x} x \right) \sin \left(k_{m_y} y \right) \,. \tag{66}$$

In practice, the response needs to be determined for only a finite number of modes as follows:

$$w = \sum_{M_{min}}^{M_{max}} \sum_{N_{min}}^{N_{max}} w_{m_x m_y} \sin\left(k_{m_x} x\right) \sin\left(k_{m_y} y\right) . \tag{67}$$

The minimum and maximum values must be chosen to include all the modes that contribute to the response of the plate in the frequency range of interest.

In order to assess reasonable values of M_{max} and N_{max}, a numerical analysis was performed on a prototypical SSP subjected to a harmonic excitation. The following material properties were assumed:

Elastomer layer: $E = 1.0 \times 10^6$ Pa $\quad \upsilon = 0.49 \quad \rho = 1200$ kg/m^3

Steel support: $E = 2.1 \times 10^{11}$ Pa $\quad \upsilon = 0.3 \quad \rho = 7900$ kg/m^3 .

The forcing function was taken as

$$P = \sin k_x x \, e^{j\omega t} , \tag{68}$$

where $k_x = 25$ m^{-1} and $f = \frac{\omega}{2\pi} = 1500$ Hz .

The computed normal displacement is shown in Figs. 6 and 7, taking into account the 10, 73, and 886 modes that most contribute to the radiation impedance. In this case, the radiation impedance has been computed numerically using Sandman's technique. It appears that about 73 modes are required to model the essentials of the flexural response of the SSP. The modes that make the largest contributions are those that have both resonant frequencies and wave numbers that nearly match the excitation. It appears possible to obtain an accurate description of the flexure by keeping only the modes having relative contributions higher than one percent.

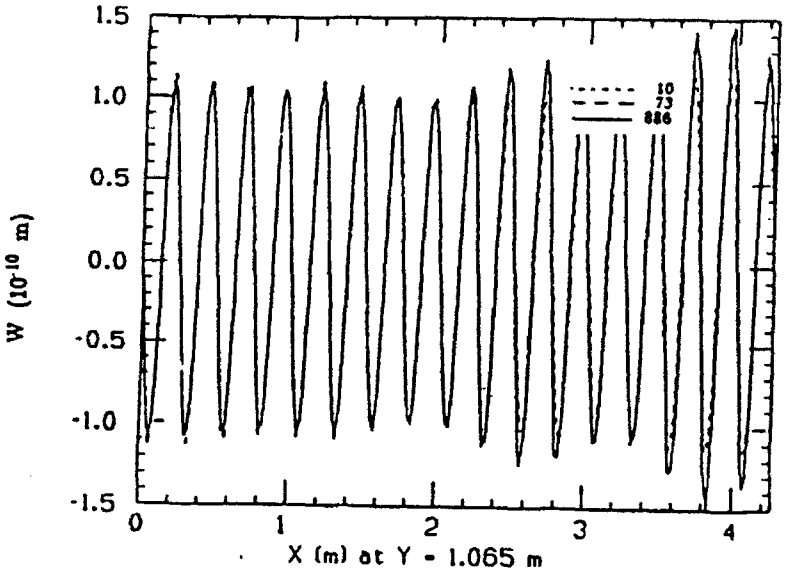

Fig. 6. - The normal displacement of the plate at y = 1.065 m computed with varying numbers of modes

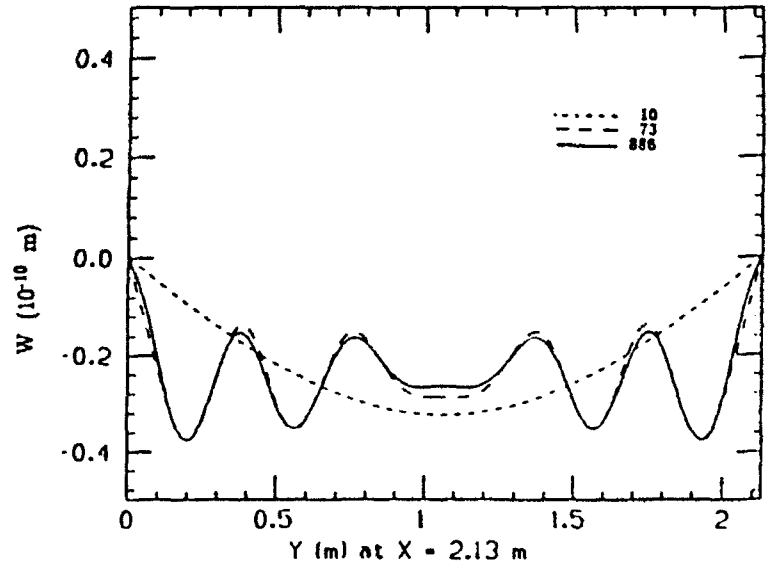

Fig 7. - The normal displacement of the plate computed at x = 2.13 m with varying numbers of modes

Finally, the flexural response as computed with the radiation impedance from Sandman's [11] numerical technique was compared to a similar result using Junger and Feit's [10] approximate formula. Figures 8 and 9 compare the results of these two methods for two representative sections through the plate; one parallel to the x axis, the other parallel to the y axis. The two methods give essentially the same results; i.e., the differences are less than the resolution of the plots. These results support the use of the simpler Junger and Feit expression for the purposes of modeling the TBL excitation of the SSP. The additional developments that follow will assume the Junger and Feit model is being employed; however, these could be generalized in a straightforward way to include Sandman's model for the water loading. Modal coupling, should it be important, could also be accommodated, but the numerical computations would become much more difficult.

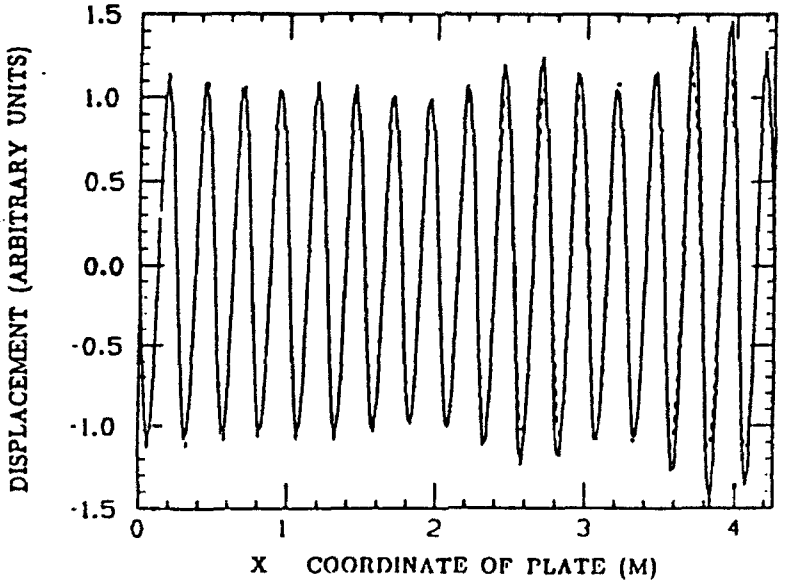

Fig. 8 - The normal displacement at y = 1.065 m computed with the Junger and Feit radiation term, compared with the more exact expression of Sandman

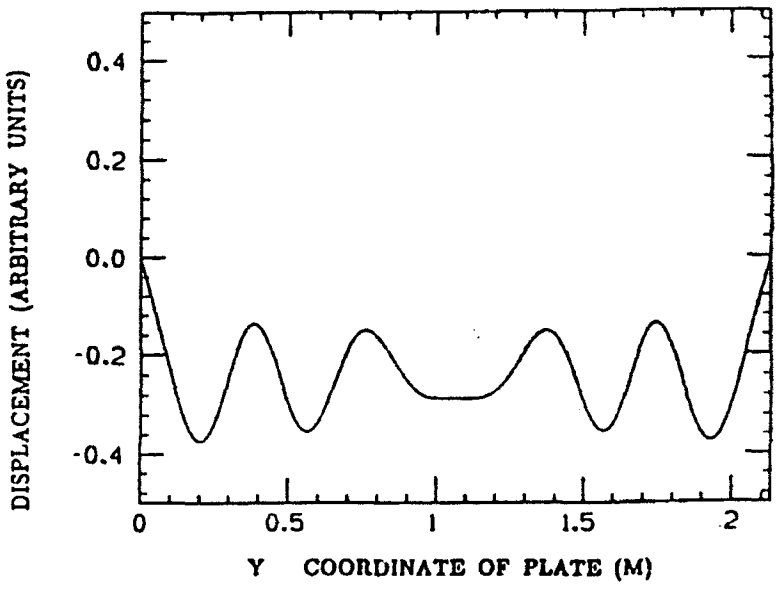

Fig. 9 - The normal displacement at x = 2.13 m computed with the Junger and Feit radiation terms, compared with the more exact expression of Sandman

Recall from the structure of Eq. (35) that the double summation over modes introduces an additional type of modal coupling into the problem. Thus, one could have two types of modal coupling: (1) via the water loading on the plate, and (2) via the double summation in Eq. (35) which arises from crosscorrelations between modes. We have argued above that the first kind of modal coupling is negligible for our problem. We shall see that the second kind is also negligible.

The Modal Frequency Response Function

The frequency response function $H_m(\omega)$ is, by definition, the complex modal amplitude w_m when the applied excitation is a unit modal force [18] given by

$$F_m = \frac{4}{L_x L_y} \sin \frac{m_x \pi x}{L_x} \sin \frac{m_y \pi y}{L_y} . \tag{69}$$

The first factor serves only as a convenient normalization factor. For a composite panel, fluid loaded on one face, pressure-released on the other face, we have already shown the following relationship between modal force and modal displacement [see Eq. (65)]:

$$\left[D_{11} \left(k_{m_x}^4 + k_{m_y}^4 \right) + 2 \left(D_{12} + 2D_{66} \right) k_{m_x}^2 k_{m_y}^2 - \rho\omega^2 - \frac{i\rho_f \omega^2}{\sqrt{k_a^2 - k_{m_x}^2 - k_{m_y}^2}} \right] w_{m_x m_y} = q_{m_x m_y} . \tag{70}$$

So, for the excitation of Eq. (69), $q_{m_x m_y} = \frac{4}{L_x L_y}$. Therefore, by definition of FRF, we have

$$H_m(\omega) = \left[D_{11} \left(k_{m_x}^4 + k_{m_y}^4 \right) + 2 \left(D_{12} + 2D_{66} \right) k_{m_x}^2 k_{m_y}^2 - \rho\omega^2 - \frac{i\rho_f \omega^2}{\sqrt{k_a^2 - k_{m_x}^2 - k_{m_y}^2}} \right]^{-1} \frac{4}{L_x L_y} . \tag{71}$$

THE ARRAY FILTER FUNCTION

As derived previously, the eigenfunctions for a plate of dimension L_x and L_y are

$$f_m(\vec{r}) = \sin \frac{m_x \pi x}{L_x} \sin \frac{m_y \pi y}{L_y} , \tag{72}$$

where m represents a pair of modal indices (m_x, m_y) that take on integral values from 1 to ∞. From Eq. (34) we have

$$\begin{aligned} a_{mn}(\vec{r}, \vec{r}') &= \left[h_{31}^2 k_{m_x}^2 k_{n_x}^2 + h_{31} h_{32}\left(k_{m_x}^2 k_{n_y}^2 + k_{m_y}^2 k_{n_x}^2\right)\right. \\ &\quad \left. + h_{32}^2 k_{m_y}^2 k_{n_y}^2\right] f_m(\vec{r}) f_n(\vec{r}') \\ &= \left(h_{31} k_{m_x}^2 + h_{32} k_{m_y}^2\right)\left(h_{31} k_{n_x}^2 + h_{32} k_{n_y}^2\right) f_m(\vec{r}) f_n(\vec{r}') . \end{aligned} \tag{73}$$

We can perform the integration over a single sensor located in region $R_i \in (x_i, y_i; x'_i, y'_i)$ obtaining

$$\begin{aligned} \int_{R_i}\int d^2r \int_{R_i}\int d^2r' \, a_{mn} &= \left(h_{31} k_{m_x}^2 + h_{32} k_{m_y}^2\right)\left(h_{31} k_{n_x}^2 + h_{32} K_{n_y}^2\right) \\ &\times \left[\frac{\cos k_{m_x} x'_i - \cos k_{m_x} x_i}{k_{m_x}}\right] \times \left[\frac{\cos k_{m_y} y'_i - \cos k_{m_y} y_i}{k_{m_y}}\right] \\ &\times \left[\frac{\cos k_{n_x} x'_i - \cos k_{n_x} x_i}{k_{n_x}}\right] \times \left[\frac{\cos k_{n_y} y'_i - \cos k_{n_y} y_i}{k_{n_y}}\right] . \end{aligned} \tag{74}$$

By summing over all regions R_i occupied by sensors we obtain the total array filter function.

THE MODAL SPECTRAL DENSITY OF THE EXCITATION

Before evaluating $\Phi_{p_{mn}}(\omega)$ it will first be necessary to evaluate the form factors $S_m(\vec{k})$, which are the Fourier transforms of the mode shapes; i.e.,

$$S_m(\vec{k}) \equiv \int\int_{A_p} e^{-i\,\vec{k}\cdot\vec{r}} \sin\left[k_{m_x} x\right] \sin\left[k_{m_y} y\right] dx\, dy \ , \tag{75}$$

where A_p denotes integration over the surface of the composite SSP. This integration can easily be done by parts, yielding

$$S_m(\vec{k}) = \frac{k_{m_x}\left\{1 - \exp\left[-i\left(k_x L_x - m_x \pi\right)\right]\right\}}{k_{m_x}^2 - k_x^2} \; \frac{k_{m_y}\left\{1 - \exp\left[-i\left(k_y L_y - m_y \pi\right)\right]\right\}}{k_{m_y}^2 - k_y^2} \ . \tag{76}$$

The power spectral density of the excitation $\Phi_{pp}(\vec{k}, \omega)$ will be represented by the Corcos [9] model

$$\phi_{pp}(\vec{k}, \omega) = \frac{P(0,\omega)\left[\alpha_1 \alpha_2 k_c^2\right]}{\left\{\pi^2\left[\left(k_x - k_c\right)^2 + \left(\alpha_1 k_c\right)^2\right]\left[k_y^2 + \left(\alpha_2 k_c\right)^2\right]\right\}} \ , \tag{77}$$

where $k_c \equiv \omega/U_c$ and U_c is the convection velocity. In addition,

$$P(0,\omega) \equiv a_+ (1+\gamma)\, \rho_f^2\, V_*^4 / \omega \ ,$$

where ρ_f is the water density and V_* is the friction velocity. The other terms a_+, γ, α_1, and α_2 are empirically determined constants.

We shall first evaluate the diagonal terms of $\Phi_{p_{mn}}(\omega)$; that is, those terms for which m = n. In this case, we can combine Eqs. (33),

(76), and (77) to obtain

$$\phi_{p_{mm}}(\omega) = \phi_{p_{m_x}}(\omega)\ \phi_{p_{m_y}}(\omega)\ \beta\ (k_c)\ , \tag{78}$$

where

$$\phi_{p_{m_x}}(\omega) \equiv 2 \int_{-\infty}^{\infty} \frac{k_{m_x}^2 \left[1 - \cos\left(k_x L_x - m_x \pi\right)\right] dk_x}{\left(k_x^2 - k_{m_x}^2\right)^2 \left[\left(k_x - k_c\right)^2 + \left(\alpha_1 k_c\right)^2\right]}, \tag{79}$$

$$\phi_{p_{m_y}}(\omega) \equiv 2 \int_{-\infty}^{\infty} \frac{k_{m_y}^2 \left[1 - \cos\left(k_y L_y - m_y \pi\right)\right] dk_y}{\left(k_y^2 - k_{m_y}^2\right)^2 \left[k_y^2 + \left(\alpha_2 k_c\right)^2\right]}\ , \tag{80}$$

and

$$\beta(k_2) \equiv P(0,\omega)\ \frac{\alpha_1\ \alpha_2\ k_c^2}{\pi^2} \tag{81}$$

Consider Eq. (79). This integral can be written as

$$\phi_{p_{m_x}}(\omega) = \text{Real}\left\{ \int_{-\infty}^{\infty} \frac{2\ k_{m_x}^2 \left[1 - e^{i\left(ZL_x - m_x\pi\right)}\right]\ dZ}{\left(Z-k_{m_x}\right)^2\left(Z+k_{m_x}\right)^2 \left[Z-k_c(1+i\alpha_1)\right]\left[Z-k_c(1-i\alpha_1)\right]} \right\}\ , \tag{82}$$

where the variable of the integration has been replaced by complex number Z. This integral may be evaluated using the contour shown in Fig. 10a. The numerator has been replaced by the real part of an exponential in order to avoid a pole where the C_∞ contour intersects the imaginary axis. There are simple poles at $-k_{m_x}$ and $+k_{m_x}$, and a second-order pole at $Z=k_c(1+i\alpha_1)$. Using the theorem of residues, we find the following results:

$$\phi_{p_{m_x}}(\omega) = \text{Real}\left\{2\pi\, k_{m_x}^2 \frac{1 - \exp i\left[k_c L_x\left(1+i\alpha_1\right) - m_x\pi\right]}{\alpha_1 k_c\left[k_c^2\left(1+i\,\alpha_1\right)^2 - k_{m_x}^2\right]^2}\right\} \tag{83}$$

$$+ \frac{\pi L_x}{2}\left[\frac{1}{\left(k_{m_x}+k_c\right)^2 + \left(\alpha_1 k_c\right)^2} + \frac{1}{\left(k_{m_x}-k_c\right)^2 + \left(\alpha_1 k_c\right)^2}\right] .$$

The expression for $\phi_{p_{m_x}}(\omega)$ can be evaluated in a similar fashion, the only difference being that the second order pole will be located on the imaginary axis. The result is

$$\phi_{p_{m_y}}(\omega) = 2\pi\, k_{m_y}^2 \frac{1 - \exp\left(-\alpha_2 k_c L_y\right)\cos m_y\pi}{\alpha_2 k_c\left[\alpha_2^2 k_c^2 + k_{m_y}^2\right]^2} \tag{84}$$

$$+ \frac{\pi L_y}{\left[k_{m_y}^2 + \left(\alpha_2 k_c\right)^2\right]} .$$

This completes the evaluation of $\phi_{p_{mn}}(\omega)$ for the diagonal terms $m = n$.

The analogous expressions for the off-diagonal terms ($m \neq n$) are

$$\phi_{p_{m_n}}(\omega) = \phi_{p_{m_x}}(\omega)\,\phi_{p_{m_y}}(\omega)\,\beta(k_c) , \tag{85}$$

where

$$\phi_{p_{m_x}} \equiv k_{m_x} k_{n_x} \int_{-\infty}^{\infty} \frac{\left[1 - e^{-i\left(k_x L_x - m_x\pi\right)}\right]\left[1 - e^{i\left(k_x L_x - n_x\pi\right)}\right] dk_x}{\left(k_x^2 - k_{m_x}^2\right)\left(k_x^2 - k_{n_x}^2\right)\left[\left(k_x - k_c\right)^2 + \left(\alpha_1 k_c\right)^2\right]} \tag{86}$$

and

$$\phi_{p_{m_y}} \equiv k_{m_y} k_{n_y} \int_{-\infty}^{\infty} \frac{\left[1 - e^{-i\left(k_y L_y - m_y \pi\right)}\right]\left[1 - e^{i\left(k_y L_y - n_y \pi\right)}\right] dk_y}{\left(k_y^2 - k_{m_y}^2\right)\left(k_y^2 - k_{n_y}^2\right)\left[k_y^2 + \left(\alpha_2 k_c\right)^2\right]} \quad . \tag{87}$$

These expressions are similar to the previous ones except that there are now four simple poles on the real axis (see Fig. 10b), and the off-axis poles are now simple poles. The evaluation is straightforward if one writes the numerator as $1 + e^{i\left(m_x - n_x\right)\pi} - e^{i\left(k_x L_x - n_x \pi\right)} - e^{-i\left(k_x L_x - m_x \pi\right)}$. The first three terms may be integrated using the upper contour in Fig. 10b, whereas the fourth term may be integrated using the lower contour. The results will not be presented because they are at least two orders of magnitude smaller than the diagonal terms for the problem of interest. This is to be expected, for upon examination of Eq. (33) it is seen that when $\Phi_{pp}(\vec{k},\omega)$ is a slowly varying function of $\vec{k}$ (as compared to S_m and S_n), then the contributions from the orthogonal form factors S_m and S_n^* tend to cancel upon integration. Thus, the cross terms are negligible except when L_x and L_y are so small that S_m and S_n vary as slowly as $\Phi_{pp}(\vec{k},\omega)$. Even if this were not the case, the off-diagonal terms in the array filter function are small for the problem of interest. A numerical study of the off-diagonal terms indicates that they are typically eight orders of magnitude smaller than the diagonal terms. The largest contributions from off the diagonal are terms for which three of the indices m_x, m_y, n_x, and n_y are equal, and the fourth index is only slightly different from the others. In such cases, the off-diagonal contribution is at least two orders of magnitude smaller than the diagonal terms.

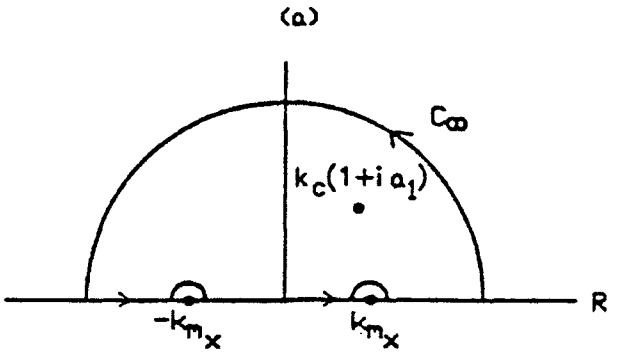

Fig. 10 (a) - Contour of integration for Eq. (82)

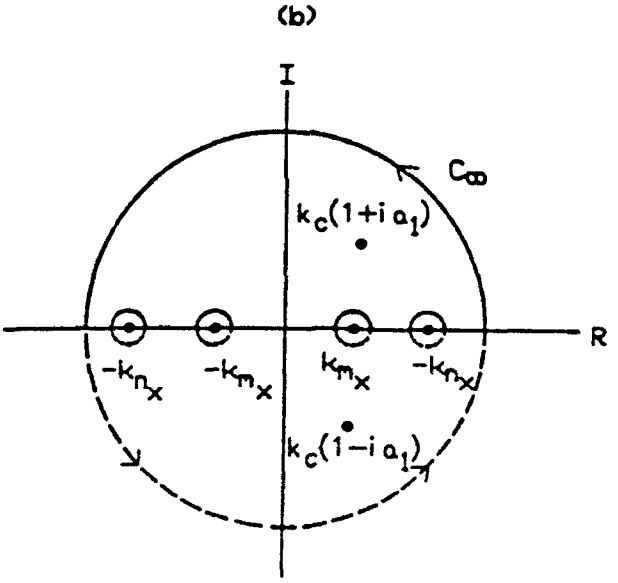

Fig. 10 (b) - Contour of integration for Eq. (86)

Now consider the product $H_m(\omega)\ H_n^*(\omega)$. The diagonal terms have peaks at frequencies where the real part of the FRF goes to zero. Fig. 11 shows some cases for light damping. At the FRF resonance frequencies the major contribution to the modal sum comes from only one mode. In the case of heavy damping the Q of these resonances is greatly reduced; thus, more than

one mode may contribute. Even so, the number of modes that need to be retained is not large because only nearest neighbors contribute at that frequency. For example, as seen from Fig 11, it is evident that to compute $\Phi_{pp}(\omega)$ at about 1.25 kHz one needs only to retain modes that have indices clustered about mode $m_x = m_y = n_x = n_y = 12$. Exclusion of the other modes greatly reduces the computational complexity of Eq. (33).

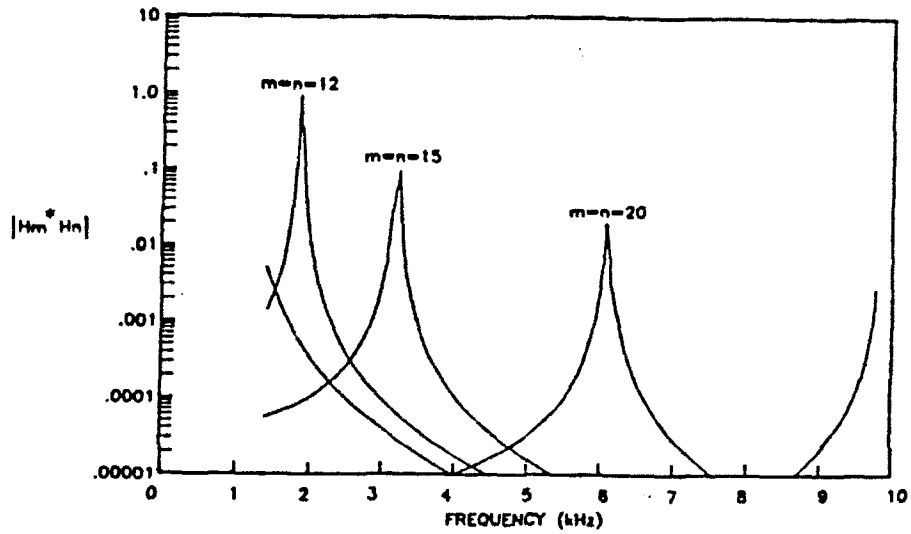

Fig. 11 - Frequency response function for several modes for which m = n

A representative plot of off-diagonal terms $H_m(\omega)\ H_n^*(\omega)$ is presented in Fig. 12. It is seen that the off-diagonal terms may have peaks at an FRF resonance frequency, but the amplitudes of the off-diagonal terms are still at least one order of magnitude smaller than the diagonal terms.

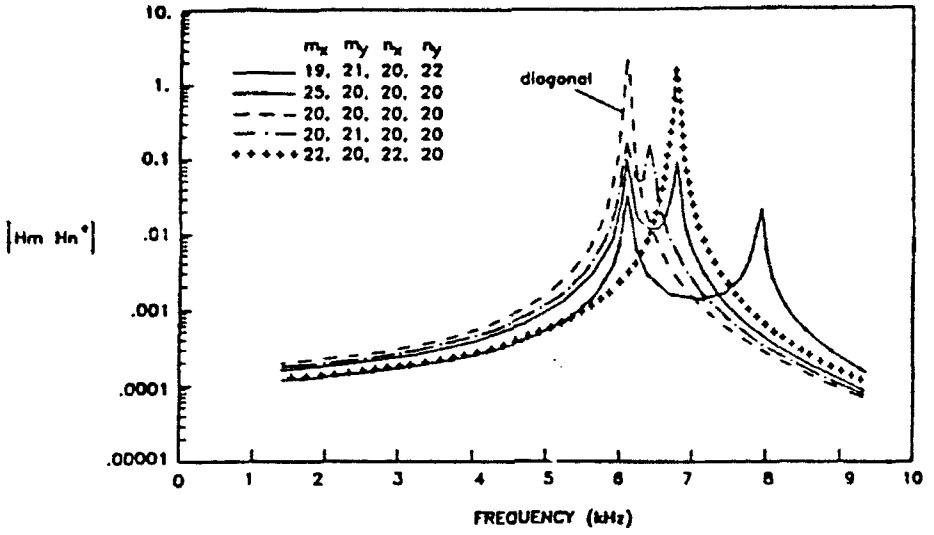

Fig. 12 - Comparison of FRF diagonal terms with FRF off-diagonal terms

NUMERICAL PROCEDURES

Because the largest values of the product $H_m(\omega)\ H_n^*(\omega)$ occur at the resonances of the FRF, an upper bound on $Q(\omega)$ can be found by evaluating Eq. (35) at those frequencies alone. Only a few modes about each resonance need to be retained in the summation. Additionally, the off-diagonal contributions of each term in Eq. (35) are at least two orders of magnitude less than the diagonal terms. Therefore, the product

$$H_m(\omega)\ H_n^*(\omega)\ \phi_{p_{mn}}(\omega) \int\int a_{mn}\ dxdy \tag{88}$$

is at least six orders of magnitude less for $m \neq n$, than for $m = n$. Therefore, no off-diagonal terms need to be retained.

The following procedure was used to evaluate Eq. (33). First, the resonances of the FRF in the frequency range of interest were determined. There are about 20 such resonances for the cases studied. For each of

these resonant frequencies $\Phi_{pp}(\omega)$ was computed by summing over 100 of the nearest neighbor diagonal terms. Some results and conclusions follow.

RESULTS

As indicated previously, the spectral density $\Phi_{pp}(\omega)$ represents the equivalent-plane-wave pressure sensed by the array. In this form $Q(\omega)$ can be directly compared to sea states and also to specifications for flow noise. Three specific cases have been studied numerically. All three cases are dual layer laminations consisting of a SSP and an elastomer of 0.051 m (the OD). The stiffness and mass of the sensor are not included. This is done to obtain relative comparisons that do not depend on the specific properties of the sensor. Thus, the three cases differ only in terms of the properties of the SSP. Figure 13 shows the results for a 0.0254 m steel SSP and a 0.0191 m glass fiber plate. Two values of loss tangent were used for the glass fiber SSP to show the influence of damping. The smaller value is more representative of practical materials.

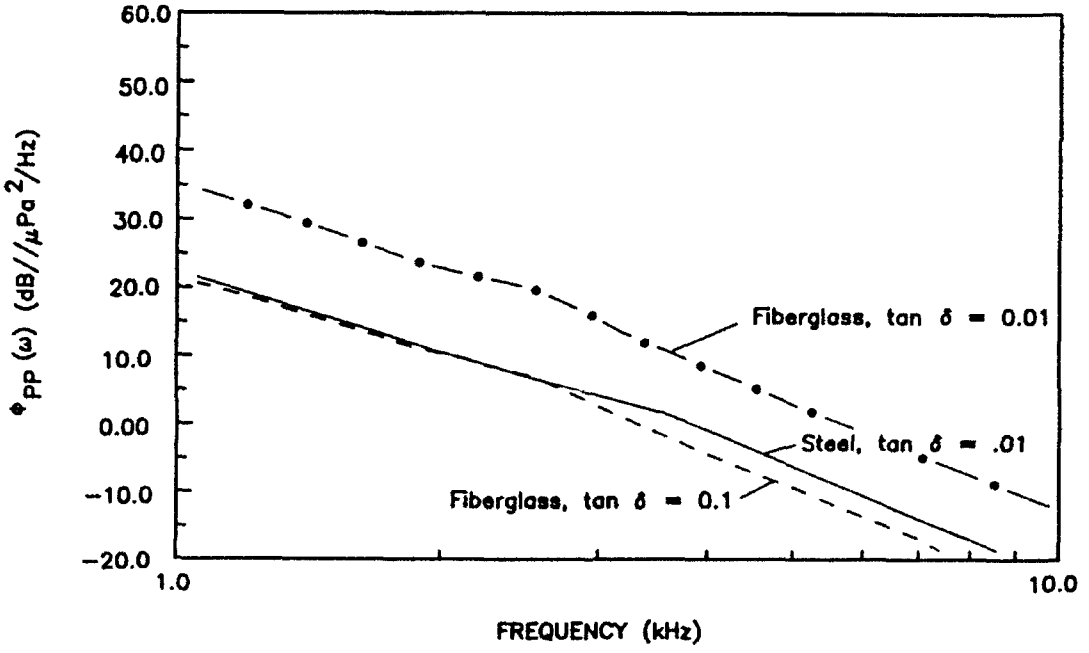

Fig. 13 - Spectral density for flexural noise induced into support plates of various compositions

CONCLUSIONS

The results indicate that a 0.0254 m steel SSP of light damping and a 0.191 m glass fiber SSP of heavy damping will both perform satisfactorily. However, the glass fiber SSP with light damping may exceed many flow noise specifications. It is also seen that flexural noise rises as frequency decreases. Therefore, flexural noise arising from THL excitations must be considered if the array is to be used at lower frequencies.

The results presented here do not account for sensor material properties or for the effects of the inner decoupler (ID). This was done for two reasons. First, the properties of the sensor and inner decoupler vary with array performance requirements. In addition, it was considered prudent to first exercise the model for a worst-case scenario in order to determine the severity of a potential noise source. The added stiffness, mass, and damping contributed by the sensor and the ID will lower the predicted noise levels. Therefore, the results represent upper limits on flexural noise for the various types of SSP's. Inclusion of the sensor in the analysis is a straightforward process if its properties are known. However, to include the ID, more analytical development will be required.

One can draw a number of conclusions about flexural noise from an examination of Eqs. (64), (67), and (73) without actually performing numerical computations. To minimize flexural noise, one should:

- Minimize d, the distance from the midplane of the SSP to the mid plane of the sensor.
- Maximize g_h/h_{12} and g_h/h_{13}, the ratios of the hydrostatic sensitivity to the lateral sensitivities.
- Maximize the number of sensors in the array and the lateral dimensions of the SSP.

- Minimize the gap between sensors. We see from Eq. (67) that if the gaps were closed in at least one dimension, then there would be essentially no noise due to flexure of the sensors. However, noise would still be radiated into the water by the edges of the SSP.

- Locate the neutral axis of the flexure at the midplane of the sensor. For example, the piezorubber or Polyvinlidene deflouride (PVDF) type sensors could be mounted on both sides of the SSP. Then, their flexural responses would cancel. However, other noise sources such as direct path flow noise and hull noise would be enhanced by such a design.

SUMMARY

Large-area, hull-mounted conformal sonar arrays are evolving in the direction of less weight and reduced hull standoff. These new array designs employ lightweight, flexible, planar sensors and lightweight support plates. Increased levels of flow-induced flexural noise may be one undesirable consequence of replacing heavier, stiffer components with lightweight, flexible components. Models exist for the radiated component of flexural noise. In this report, a model is developed that accounts for a heretofore neglected flexural noise mechanism; i.e., direct coupling of the flexure with the lateral displacement of a planar sensor. The development of the model was presented for piezoelectric sensors such as rubber-lead titanate composites and PVDF; however, the development could be adapted to consider other sensor types such as fiber optic sensors. The expression derived for the spectral density arising from this model [Eq. (35)] has terms of which some are analogous to the expression for the direct path spectral density [Eq. (11)]. On the other hand, some terms in Eq. (35) are unique; these account for the modal response of the plate and intermodal coupling arising from fluid loading as well as cross-modal correlations.

Some perspectives on the model, and its implementation, were presented for one particular array configuration that approximates arrays of practical interest. The support plate with sensors and inner decoupler was represented as a thin, finite, composite plate, water loaded on the sensor

side and pressure relieved on the opposite face. The water loading was modeled with an approximate expression derived by Junger and Feit [10]. The validity of these assumptions and approximations was demonstrated by comparing the approximated resonances and displacements with values obtained by more exact models.

An exact analytical expression for the spectral density of flexural noise was derived for the case where the random excitation field is characterized by the Corcos model. In general, this expression involves a quadruple summation, each to infinity, over the normal modes of the plate. However, it was shown that only a few modes need to be included for each frequency of interest. Therefore, the model is easily tractable for practical applications.

Finally, the sensitivity of the spectral density to various array parameters was presented. The parameters of influence include the piezoelectric constants of the sensors, the sensor standoff distance, the material constants of the support plate, and the size and spacing characteristics of the array.

Most of the limiting assumptions of the model could be addressed without modifying the basic approach. For example, if the assumption of a pressure-release backing to the support plate is not valid for a given application, then one could employ a boundary condition that specifies a known impedance which might represent, for example, an ID placed between the support plate and the hull of the ship. Another limiting assumption is that the structure behaves as a thin plate. This assumption manifests itself in the model via the relationships between lateral strains and the normal displacement [Eq. (2)]. This limitation may be removed by replacing Eq. (2) with analogous expressions obtained from thick plate theory.

The results of this report provide an analytical approach and a mathematical expression for the noise induced in an array of extended sensors that derives from the coupling of the lateral sensitivity of the sensor to the flexure of the support structure.

REFERENCES

1. J. E. Cole, "Array Noise From Vibration of The Signal Conditioning Plate," TM/U-1495-362, Cambridge Acoustical Associates, Inc, Cambridge, MA, 28 April 1987.

2. W. A. Strawderman, "Turbulence-induced plate vibration: An evaluation of finite- and infinite-plate models," *J. Acous. Soc. Am.* 46(5), pt. 2, pp. 1294-1307 (1969).

3. W. A. Strawderman and R. A. Christman, "Turbulence-induced plate vibrations: Some effects of fluid loading on finite and infinite Plates," *J. Acous. Soc. Am.* 52(5), pt 2, pp. 1538-1552 (1972).

4. R. A. Christman, "Pressure Radiated by Turbulence-Excited Finite and Infinite Water-Loaded Plates," TR4573, Naval Underwater Systems Center, New London, CT, 4 Oct. 1973.

5. K. L. Chandiramani, "Vibration response of fluid-loaded structures to low-speed flow noise," *J. Acous. Soc. Am.* 61(6), pp. 1460-1470 (1977).

6. K. L. Chandiramani, "Response of underwater structures to convection component of flow," *J. Acous. Soc. Am.* 73(3), pp. 835-839 (1983).

7. D. Chase, "Some Model Results in Classical Hydrodynamics," TM 51, Chase, Inc., Boston, MA, 18 Dec. 1986.

8. Y. B. Semenenko, "Sound Radiation From a Thin Semi-Infinite Plate Driven By a Turbulent Boundary Layer, *Sov. Phys. Acous.* 36(6), pp. 601-604 (Nov-Dec 1990).

9. G. M. Corcos, "The Structure of The Turbulent Pressure Field in Boundary Layer Flows," *J. of Fluid Mechanics* 18, pp. 353-378 (1964).

10. M. C. Junger and D. Feit, *Sound, Structures and Their Interactions*, 2nd ed. (MIT Press, Cambridge, MA, 1972), Ch. 8.

11. B. E. Sandman, "Motion of a three layered elastic-viscoelastic plate under fluid loading," *J. Acous. Soc. Am.* 57(5) pp. 1097-1107(1975).

12. D. Ricketts, "Transverse vibrations of composite piezoelectric polymer plates," *J. Acous. Soc. Am.* 77(5), pp. 1939-1945 (1987).

13. W. P. Mason, "Use of Piezoelectric Crystals and Mechanical Resonators in Filters and Oscillators," in *Physical Acoustics*, W. P. Mason, ed. (Academic Press, New York, NY, 1904), Vol. 1 - Part A, Ch. 5.

14. W. K. Blake, *Mechanics of Flow-Induced Sound and Vibration*, 1st ed. (Academic Press, Orlando, FL, 1986), Vol. II, pp. 562-569.

15. D. M. Chase and R. Stern, "Turbulent-Boundary-Layer Transmitted Into an Elastic Layer," BBN Tech. Memo. 382, Bolt, Beranek and Newman, Inc., Cambridge, MA, 1977.

16. P. H. White, "Effect of transducer size, shape and surface sensitivity on the measurement of boundary-layer pressures," *J. Acous. Soc. Am.* 41(5), pp. 1358-1363 (1967).

17. S. H. Ko and H. H. Schloemer, "Calculations of turbulent boundary layer pressure fluctuations transmitted into a viscoelastic layer," *J. Acous. Soc. Am.* 85(4), pp. 1469-1477 (1989).

18. Y. K. Lin, *Probalistic Theory of Structural Dynamics* (Robert Krieger Publishing Co., Huntington, NY, 1976), Ch. 7.

19. S. B. Dong, "Free vibration of laminated orthotropic cylindrical shells," *J. Acous. Soc. Am.* 44(6), pp. 1628-1635 (1968).

20. A. W. Leissa, "Vibrations of Shells," NASA SP-288, National Aeronautics and Space Administration, Washingon, DC, pp. 158-159, 1973.

21. S. Timoshenko and S. Woinowsky-Krieger, *Theory of Plates and Shells*, 2nd ed. (McGraw-Hill Book Co., New York, NY, 1959), p. 108.

22. A. Harari and B. E. Sandman, "Radiation and vibrational properties of submerged stiffened cylindrical shells," *J. Acous. Soc. Am.* 88(4), pp. 1817-1830 (1990).

23. G. Maidanik, "The Influence of Fluid Loading on the Radiation from Orthotropic Plates," *J. Sound Vib.* 3, pp. 288-299 (1966).

24. R. A. Mangiarotty, "Acoustic radiation damping of vibrating structures," *J. Acous. Soc. Am.* 35, pp. 369-377 (1963).

25. G. Maidanik and E. M. Kerwin, "Influence of fluid loading on the radiation from infinite plates below the critical frequency," *J. Acous. Soc. Am.*, 40, pp. 1034-1038 (1966).

26. H. G. Davies, "Sound from turbulent-boundary-layer - excited panels," *J. Acoust. Soc. Am.*, 49, pp. 878-889 (1971).

27. R. C. Leibowitz, "Methods for Computing Radiation Damping and The Vibratory Response of Fluid Loaded and Acoustically Radiating Finite Rectangular Plates Subject to Turbulence Excitation - Option 4," David Taylor Naval Ship R&D Center Report 2976D, Mar. 1972.